

Pretransitional effects near the smectic-A–smectic-C* phase transition of hydrophilic and hydrophobic aerosil networks dispersed in ferroelectric liquid crystals

George Cordoyiannis,^{1,2} Samo Kralj,^{3,2} George Nounesis,^{1,*} Zdravko Kutnjak,² and Slobodan Žumer^{4,2}

¹National Centre for Scientific Research “Demokritos,” 153 10 Aghia Paraskevi, Greece

²Jožef Stefan Institute, P.O. Box 3000, 1001 Ljubljana, Slovenia

³Laboratory of Physics of Complex Systems, Faculty of Education, University of Maribor, Koroška 160, 2000 Maribor, Slovenia

⁴Department of Physics, Faculty of Mathematics and Physics, University of Ljubljana, Jadranska 19, 1000 Ljubljana, Slovenia

(Received 16 June 2006; published 6 February 2007)

A detailed x-ray scattering and high-resolution ac calorimetric study has been carried out near the smectic-A to chiral smectic-C phase transition of liquid-crystal compounds 4-(2-methyl butyl) phenyl 4-*n*-octylbiphenyl-4-carboxylate (CE8) and *p*-(*n*-decyloxy) benzylidene-*p*-amino-(2-methylbutyl) cinnamate (DOBAMBC) confined in hydrophilic and hydrophobic aerosil nanoparticle networks. The character of the transition, which is mean field near a tricritical point in bulk, is changed dramatically with an increase of aerosil-induced disorder. X-ray measurements revealed pretransitional behavior and compression of the smectic layers, phenomena that are strongly pronounced in high aerosil concentrations. A theoretical model that takes into account the interplay of relevant mechanisms is proposed to explain the observed phenomena. The effect of chirality on the interaction of liquid crystals with aerosils is discussed.

DOI: 10.1103/PhysRevE.75.021702

PACS number(s): 61.30.-v, 65.20.+w, 61.10.-i

I. INTRODUCTION

The past decade has evidenced a rapidly increasing interest in mixtures of liquid crystals (LCs) with aerosil spherular particles [1–6]. These mixtures constitute experimental model systems to study the influence of random-type disorder on the behavior of phases with a broken continuous symmetry. By changing the mass density ρ_a of the aerosil particles, at least three qualitatively different random field regimes experienced by the LC molecules are encountered [2,3]. In the *dilution* regime ($\rho_a < 0.01$ g/cm³), the aerosil particles almost independently float in the liquid LC environment ($\rho_a = m_a/V_{lc} = m_a\rho_{lc}/m_{lc}$, where m_a stands for the mass of silica particles, while m_{lc} , V_{lc} , and ρ_{lc} stand for the mass, volume, and density of LC, respectively). For $0.01 < \rho_a < 0.1$ g/cm³, the aerosil particles form a responsive gel-like structure, which characterizes the *soft* regime. Consequently, the LC phases experience partially annealed random field-type disorder. The aerosil network can rearrange in order to partially relax the local elastic stress by the LC component. For $\rho_a > 0.1$ g/cm³, the *stiff* regime is entered. The aerosil network forms a rigid structure that enforces upon the LC a quenched random field-type disorder.

In addition, these systems are of great interest for the physics of adaptive networks [7]. In the language of network physics, the *diluted*, *soft*, and *stiff* regimes correspond to the so called *floppy*, *intermediate*, and *rigid* network configuration [8], respectively. LC-aerosil mixtures are also of interest for their potential for various electro-optical applications, particularly due to their gray-scale capabilities.

The initial studies mainly focused on the influence of aerosil particles on the isotropic to nematic (*I-N*) and nematic to smectic-A (*N-Sm-A*) phase transitions [2,3,9–18]. One of the important findings of these studies is that the presence

of aerosils presumably destroys the quasi-long-range smectic ordering [1,19]. The pseudophase transition-temperature shifts exhibit in general nonmonotonous behavior as a function of ρ_a [2,18,20]. High-resolution calorimetric measurements at the *N-Sm-A* phase transition clearly reveal finite-size effects [17]. Furthermore, with increased ρ_a the coupling between the nematic and smectic order parameter is decreased [9] leading to three-dimensional (3D) *XY*-like behavior on approaching the *stiff* regime [2].

Studies on the phase behavior across the smectic-A to smectic-C (*Sm-A-Sm-C*) or smectic-A to chiral smectic-C (*Sm-A-Sm-C**) phase transitions have also been reported recently [5,21–29]. The dielectric studies [21,22] on chiral CE8 liquid crystal reveal that the Goldstone mode exhibits bulklike response for $\rho_a < 0.1$ g/cm³ and vanishes for $\rho_a > 0.1$ g/cm³. On the other hand, the soft mode shows dramatic changes in the behavior for all ρ_a in comparison with the pure bulk sample. This is expected to be due to local variations in smectic layer spacing. The latter prediction is in line with recent x-ray scattering measurements [5]. These studies also indicate that the aerosil network enforces a finite tilt of LC molecules with respect to the smectic layer normal even in the *Sm-A* phase. However, this behavior was not observed in nonchiral $\bar{8}S5$ samples [23] in which pure bulklike features were observed even for $\rho_a > 0.1$ g/cm³. This suggests that the weakly polar LC molecules experience a weaker pinning field due to the aerosil network than the strongly polar and chiral materials do. Furthermore, calorimetric studies reveal that with increasing ρ_a , the *Sm-A-Sm-C* pseudocritical heat capacity (C_p) anomaly exhibits crossover from a tricritical mean-field (MF) toward a simple steplike MF behavior [25].

Note that the presence of quenched disorder in general triggers glassy features, as minimal theoretical models (i.e., Heisenberg or Ising-type models with different origins of quenched disorder) suggest [30]. In particular, if a pure system phase suffers a loss of continuous symmetry, even an

*Electronic address: nounesis@rrp.demokritos.gr

arbitrary weak disorder breaks the long-range order of the system in spatial dimensions less than 4. This so called Imry-Ma theorem [31] also predicts that the resulting glassy phase exhibits a short-range order (SRO). Glassy features have been clearly manifested experimentally in various randomly perturbed magnetic systems [30], with the exception of the Imry-Ma prediction. Namely, it was shown latter that a weak enough disorder can give rise to a glassy phase with a quasi-long-range order (QLRO) [32,33]. The influence of quenched disorder is expected to be large in various LC phases because of their soft character and broken continuous symmetries. However, recent experimental studies in LC-aerosil mixtures report on apparent glassy features only at the I - N transition. Thermal history-dependent results were observed by Bellini *et al.* [34,35] in different cyanobiphenyl LCs by means of turbidity study, supported by Monte Carlo simulations using modified Lebwohl-Lasher [36] interaction. Care was taken that the observed memory effects were not due to the restructuring of the aerosil network. In addition, these studies confirmed the Imry-Ma prediction and SRO for LC-aerosil mixtures. Particular attention was paid to the double-peak specific-heat temperature dependence at the I - N transition [4,37,38]. It was claimed that this feature signals the transition from the random diluted to random field regime as the temperature is lowered. Both peaks show hysteresis and frequency dependence [4,38], which is particularly pronounced for the lower-temperature peak. However, hysteretic effects have not yet been clearly observed in smectic phases [16]. The reason behind this is not yet clearly understood [4,38]. It is possible that the dynamics of the system are fast enough to find equilibrium within the experimental time. There are also speculations [38] that in the nematic phase, memory effects appear due to the pinning of topological line defects, the position of which cannot be significantly altered at lower-temperature smectic phases.

In this contribution, we present a systematic experimental and theoretical study on the influence of ρ_a of hydrophilic and hydrophobic aerosil particles on the Sm-A-Sm-C^* phase transition of the LC compounds CE8 and DOBAMBC. For comparison, measurements on the nonchiral compound 4-*n*-pentyl-phenylthiol-4'-*n*-octyloxybenzoate ($\bar{8}\text{S5}$) have also been carried out. X-ray scattering and high-resolution calorimetry were used in order to measure the smectic-layer thickness (d), the tilt angle (θ), and the heat capacity as functions of temperature and ρ_a . Specifically, we show that the smectic layer thickness exhibits anomalous compression with increasing ρ_a . The impact of the nanoparticle density is more pronounced in chiral samples, revealing a density-induced soft-stiff transition in the aerosil network. For the theoretical description, we use the Landau-Ginzburg type of phenomenological approach in order to discuss different possible origins that can influence the observed $d(\rho_a)$ dependence and related $\theta(\rho_a)$ pretransitional phenomena.

The organization of the paper is as follows. Section II consists of a brief description of sample preparation and the experimental setups. In Sec. III, the Landau-Ginzburg model is described focusing on the Sm-A-Sm-C^* phase transition. The experimental results are presented in Sec. IV followed by a theoretical analysis in Sec. V. In Sec. VI, the discussion

of experimental results is given within the frame of the model introduced in Sec. III. Finally, the conclusions are presented in Sec. VII.

II. EXPERIMENTAL PROCEDURES

Two kinds of silica nanoparticles were used as disorder agents, the hydrophilic aerosil 300 and the hydrophobic aerosil R812. They are both produced by Degussa and they are spherical in shape, with a diameter of $2R_a \sim 7$ nm and an active surface area of $a=300$ and 260 $\text{m}^2 \text{g}^{-1}$, respectively. The LC compound CE8 was supplied by Merck and was used without any additional treatment; DOBAMBC was synthesized at Jožef Stefan Institute and $\bar{8}\text{S5}$ at Kent State University.

Prior to mixing with LC, the aerosils were heated up to 700 K for drying and burning of possible organic impurities. The samples were prepared by dilution of both LC and aerosils in ultrapure acetone, using the method described in detail elsewhere [5,39]. After mixing, the samples were kept in the Sm-A phase until measurements were performed. For both x-ray and calorimetric experiments, the samples were instantly heated up to the isotropic phase, and then slowly cooled down to the smectic phases.

To define the aerosil concentration, in the mixture with LC, the temperature-independent parameter $x=m_a/(m_a+m_{lc})$ was used. Taking into account that the density of LCs is very near 1 g/cm^3 and $m_a \ll m_{lc}$ in most LC and aerosil mixtures, the values of parameters x and ρ_a are relatively close to each other. Samples of various concentrations were prepared for both CE8 ($x=0.05, 0.10, 0.12, 0.135, 0.15, 0.25$ hydrophilic and $x=0.025, 0.05, 0.15$ hydrophobic) and DOBAMBC ($x=0.03, 0.08, 0.15, 0.25$ hydrophobic) compounds. One concentration of $\bar{8}\text{S5}$ ($x=0.15$ hydrophobic) was also measured.

For x-ray measurements, the samples were placed in thin tubes (Hilgenberg-Mark tubes of 1 mm inner diameter) and were then attached to a computer-controlled heating stage by Instec Inc., with a temperature stability of ± 0.01 K. Measurements were taken at selected temperatures in both Sm-A and Sm-C^* phases. The x-ray setup consists of a Rigaku RUH3R rotating anode generator, operating at 5.4 kW and producing a beam of $\lambda=1.5416 \text{ \AA}$ (K_α line of Cu). Flat graphite was used as a monochromator. Point focusing of the beam ($0.3 \times 0.3 \text{ mm}^2$) was attained by double focusing mirrors by Molecular Structure Co, in continuous He flow. The detector was an R -axis IV double imaging plate system (area of $300 \times 300 \text{ mm}^2$) built by Molecular Structure Co. The pixel size was $100 \times 100 \mu\text{m}^2$, corresponding to a reading time of 3 min, and the sample-to-detector distance during experiments was set to 279 mm. The dynamic range of this system is 10^6 and the resolution is 0.004 \AA^{-1} (half-width at half maximum). The exposure times were adjusted from 3 min (bulk LCs) up to 10 min (high aerosil concentrations) in order to achieve a clear spectrum, even for the second-harmonic Bragg peak.

For the calorimetric measurements, the samples were placed in silver cells thermally linked to a temperature sta-

bilized bath through supportive wires and air. The ac C_p data were acquired by a computerized calorimeter. A detailed description of this technique can be found in Refs. [40–42]. In order to obtain the net C_p of the sample, the C_p of empty cell was subtracted from the raw data. Typical scan rates were 70–100 mK/h near the transition temperature and 200–400 mK/h away from it.

III. MODEL

We consider a nonchiral thermotropic LC exhibiting the continuous Sm-A–Sm-C phase transition at $T=T_c$. A simplest possible model is taken into account in order to reproduce qualitatively the observed results. We focus on equilibrium phenomena. Glassy features that might arise due to the random character of the aerosil network are not considered. The LC ordering is described with the nematic director field \vec{n} and the smectic complex order parameter $\psi = \eta e^{i\phi}$. The unit vector \vec{n} reveals the average local orientational ordering of rodlike LC molecules. The degree of smectic layering is determined by the translational order parameter η and the position of layers by the phase factor ϕ . The model we use can also well describe the chiral case. This is due to the fact that the main phase behavior features are controlled by the primary order parameter θ . The tilt-induced polarization, which is related to the chirality, plays a secondary role within this context [43].

In terms of these continuum fields, we express the free energy $F = F_v + F_i$ of the liquid crystal as the sum of volume $F_v = \int f_v d^3\vec{r}$ and the interface contribution $F_i = \int f_i d^2\vec{r}$. The first integral is carried out over the entire volume occupied by the LC phase and the second one over the LC-aerosil interface, respectively.

In the simplest approximation, we express the volume free-energy density as [44–46]

$$f_v = \frac{K}{2} |\nabla \vec{n}|^2 + C_{II} |(\vec{n} \cdot \nabla - iq_0)\psi|^2 + C_{\perp} |(\vec{n} \times \nabla)\psi|^2 + \sum_{p=1,2} D_p |(\vec{n} \times \nabla)\psi|^{2(p+1)}. \quad (1)$$

The first term in f_v enforces a homogeneous uniaxial ordering along the symmetry breaking direction given by \vec{n} , where K represents an average Frank nematic elastic constant.

The remaining terms in Eq. (1) determine the translational LC ordering. The term weighted by the compressibility smectic elastic constant C_{II} is referred to as the compressibility term. In the Sm-A phase, it tends to establish the layer periodicity given by $q_0 = 2\pi/d_0$ for \vec{n} pointing along the smectic layer normal $\vec{v}_s = \frac{\nabla\phi}{|\nabla\phi|}$. The corresponding phase factor can be expressed as $\phi(\vec{r}) = q_0 \vec{n} \cdot \vec{r}$. The smectic bend elastic term is weighted by the smectic bend elastic constant C_{\perp} . This constant is assumed to exhibit a linear temperature dependence close to the Sm-A–Sm-C phase transition temperature T_c . Thus

$$C_{\perp} = C_{\perp}^{(0)}(T - T_c), \quad (2)$$

where $C_{\perp}^{(0)}$ is a constant. For $T > T_c$, the smectic bend elastic constant is positive, tending to align \vec{n} along \vec{v}_s . For $T < T_c$,

in the Sm-C phase, a tilt of LC molecules with respect to \vec{v}_s is enforced due to $C_{\perp} < 0$. In Eq. (1), the terms weighted with the positive elastic constants D_1 and D_2 are introduced to stabilize the resulting cone angle $\theta = \arccos(\vec{n} \cdot \vec{v}_s)$ at $\theta < \pi/2$. By varying the relative strength of these two terms, the cases simulating either the mean-field or tricritical-like mean-field behavior are roughly reproduced. Namely, these terms are proportional to $\theta^{2(p+1)}$ for a spatially homogeneous tilt and $\theta \ll 1$.

We can express the volume part free-energy density for the homogeneous case, in which \vec{n} , η , and smectic periodicity q are spatially homogeneous and the phase factor is expressed as $\phi = q \vec{v}_s \cdot \vec{r}$. It follows that

$$f_v = \eta^2 C_{II} (q \cos \theta - q_0)^2 + \eta^2 C_{\perp} q^2 \sin^2 \theta + \eta^4 D_1 q^4 \sin^4 \theta + \eta^6 D_2 q^6 \sin^6 \theta. \quad (3)$$

By introducing new variables $y = q \cos \theta$ and $z = q \sin \theta$, we obtain

$$f_v = \eta^2 C_{II} (y - q_0)^2 + a_0 t z^2 + b z^4 + c z^6, \quad (4)$$

where $t = (T - T_c)/T_c$ is the reduced temperature, $a_0 = C_{\perp}^{(0)} T_c \eta^2$, $b = D_1 \eta^4$, and $c = D_2 \eta^6$. We minimize the free energy density for a constant value of η . The solution to the equations $\frac{\partial f_v}{\partial y} = 0$, $\frac{\partial f_v}{\partial z} = 0$ yields the following solution in the elastically undistorted Sm-C phase:

$$\psi = \eta e^{iq \vec{v}_s \cdot \vec{r}}, \quad (5)$$

$$q = q_0 \cos \theta, \quad (6)$$

$$\theta = \arctan \left[\sqrt{\frac{b q_0^2}{3c} \left(\sqrt{1 - \frac{3t}{t_0}} - 1 \right)} \right]. \quad (7)$$

The value of dimensionless parameter $t_0 = \frac{b^2}{a_0 c}$ distinguishes [47] well between the MF and tricritical MF-type behavior. The latter is realized for $t_0 \ll 1$.

The corresponding equation for the heat capacity for small values of θ reads [47]

$$C_p = \begin{cases} A \frac{T}{T_c} \left(\frac{T_m - T_c}{T_m - T} \right)^{1/2} + B + CT & \text{if } T < T_c \\ B + CT & \text{if } T > T_c. \end{cases} \quad (8)$$

Here $A = \frac{a_0^2}{2bT_c}$ is the heat capacity jump at T_c , $T_m = \left(\frac{t_0}{3} + 1\right) T_c$, and the constants C and B are considered taking into account a linear background in C_p .

In the interface free-energy contribution, we take into account only the orientational anchoring term. Using the Rapini-Papoular formula [48], we express it as

$$f_i = \frac{W}{2} [1 - (\vec{e}_s \cdot \vec{n})^2]. \quad (9)$$

The positive constant W is the surface anchoring strength and \vec{e}_s defines the surface easy axis (i.e., the surface free-energy density term is minimized if \vec{n} is aligned along \vec{e}_s). In our samples, the aerosils enforce homeotropic anchoring, for

which the LC molecules tend to be aligned along the LC-aerosil interface normal.

The main part of the analysis is carried out in the Sm-A phase where, in addition to the mean aerosil void size $l_0 \sim 2/(a\rho_a)$ [2] and the aerosil unit radius R , the following characteristic lengths can be introduced [46]: the orientational anchoring extrapolation length d_e and the penetration lengths $\lambda_{||}$, λ_{\perp} . They are conventionally expressed as

$$d_e = \frac{K}{W}, \quad (10)$$

$$\lambda_{||} = \sqrt{\frac{K}{\eta^2 q_0^2 C_{II}}}. \quad (11)$$

$$\lambda_{\perp} = \sqrt{\frac{K}{\eta^2 q_0^2 C_{\perp}}}. \quad (12)$$

A quantity of interest is also the layer compression

$$\Delta d = d_0 - d. \quad (13)$$

Here $d_0 = 2\pi/q_0$ describes the equilibrium smectic spacing as observed in bulk samples, and $d = 2\pi/q$ stands for the spacing that is measured for the LC-aerosil mixtures.

At this point, we introduce the following quantities characterizing the aerosil-LC mixture, which will be used later. The spherular aerosil particles of mass density $\rho_s \sim 2.2 \text{ g/cm}^3$ have a radius $R_a \sim 3.5 \text{ nm}$. These particles often form aggregates. We describe the average radius of such an aggregate by $R = n_a R_a$, where n_a typically ranges between 1 and 3. The quantity $N_a = m_a/M_a$ counts the number of aerosil particles in the system; M_a is the molecular mass of an aerosil particle, which occupies the volume $v_a \sim 4\pi R_a^3/3$. Taking into account that $m_a = \rho_a V$ and $M_a = \rho_s v_a$, it follows that

$$N_a \sim \frac{3V_{LC} \rho_a}{4\pi R_a^3 \rho_s} \sim \frac{3V_{LC} \rho_{LC}}{4\pi R_a^3 \rho_s} x. \quad (14)$$

IV. EXPERIMENTAL RESULTS

In this section, the results for the three LC compounds are presented, starting from the chiral CE8 and DOBAMBC. The chemical formula, phase sequence, and transition temperatures for each LC compound—CE8, DOBAMBC, and $\bar{8}S5$ —are shown in Fig. 1.

In Fig. 2(a), the normalized intensity of x-ray spectra versus the wave vector q is shown for bulk CE8 and two hydrophilic aerosil concentrations $x=0.05$ and 0.15 . In the case of the aerosil mixtures, one can observe for low q values a broad scattering peak with a maximum around 6.8 nm corresponding to the nanoparticles. With increasing q , the first- and second-harmonic quasi-Bragg smectic peaks can be clearly seen. In Fig. 2(b), the first-harmonic peaks are plotted as a function of $q - q_0$. Significant broadening is observed for both aerosil concentrations. This broadening cannot be attributed solely to the finite-size effects [5]; additional reasons have to be sought.

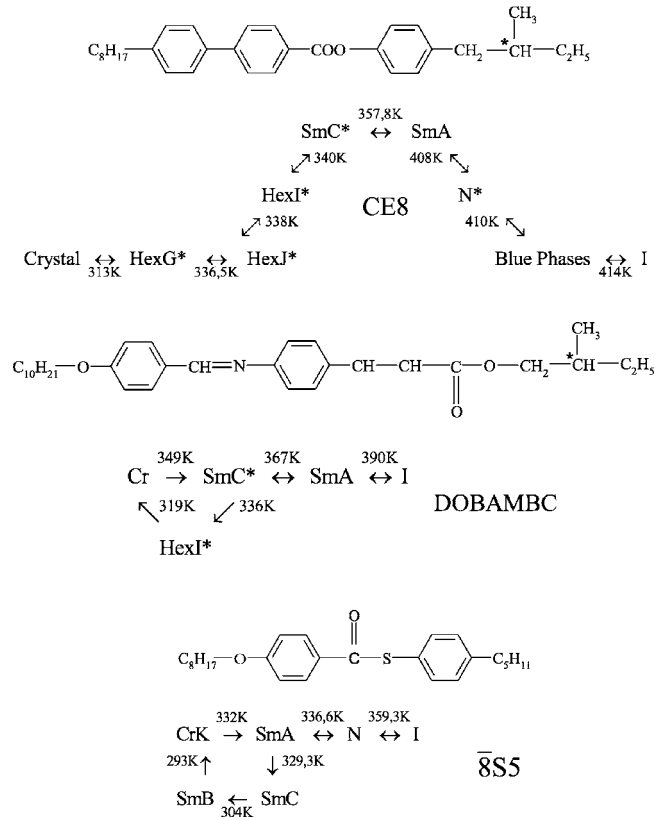


FIG. 1. The chemical formulas, phase sequences, and transition temperatures of the three liquid crystals CE8, DOBAMBC, and $\bar{8}S5$.

As shown in Fig. 3(a), the smectic layers are also compressed above the transition temperature for CE8 and hydrophilic aerosil mixtures. This pretransitional behavior in tilt angle θ becomes dramatically pronounced at high aerosil concentrations [Fig. 3(b)]. In the same figure, the solid line represents a fit of θ for bulk CE8 using the extended mean-field model [47]. The $\theta(T)$ profiles have thus been fitted using the Eq. (7) only for $x \leq 0.10$. Higher concentrations could not be adequately fitted due to extended smearing of the tilt angle data near the transition.

The character of the transition is strongly affected by the concentration of aerosils. Figure 3(b) shows the impact of concentration on the tilt angle. For high x values, the values of the tilt angle deep in the Sm-C* phase are increasingly suppressed, while above T_c the induced pretransitional molecular tilt can be detected for high temperatures in the Sm-A phase. Similar behavior was also observed for the hydrophobic mixtures, as illustrated in Fig. 4. Slight differences can be observed in the magnitude of the tilt angle suppression deep into the Sm-C* phase as well as in the width of the temperature range in which pretransitional effects are detectable.

The strong impact of aerosil-induced disorder upon the Sm-A–Sm-C* transition of CE8 is also confirmed by measurements of C_p using a high-resolution ac calorimeter. The plot of C_p versus temperature for CE8 and three hydrophilic mixtures (Fig. 5) shows the dramatic change in the shape of the transition. Similar to the order parameter θ , the C_p data

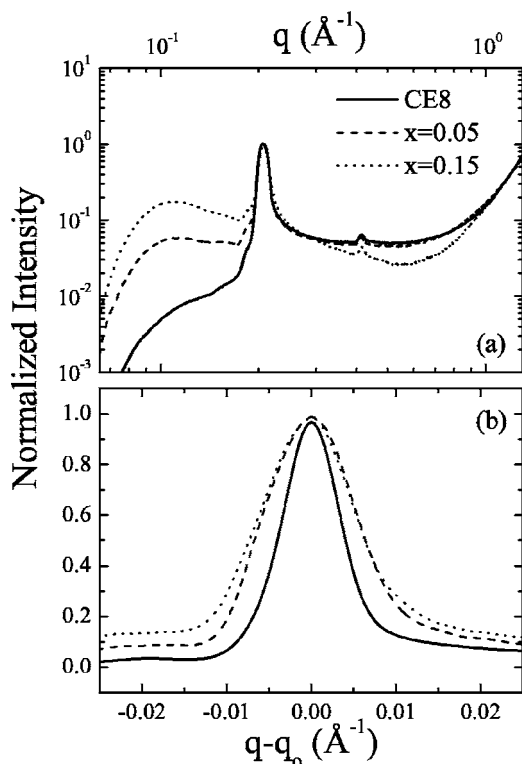


FIG. 2. (a) A wide-range x-ray spectrum of normalized intensity vs the wave vector q for CE8 bulk (solid line) and two hydrophilic aerosil mixtures $x=0.05$ (dashed line) and $x=0.15$ (dotted line) is shown. (b) The first harmonic quasi-Bragg peak for all samples is plotted versus $q - q_0$.

for bulk LC can be well fitted by using the extended mean-field ansatz (8). With increasing concentration x of hydrophilic aerosils, the C_p anomaly is strongly suppressed and increasingly smeared. As aerosil concentration is increased, the ratio b/c obtained from fits of both x-ray and C_p data increases (Table I) for both CE8 and DOBAMBC mixtures, indicating a crossover from the mean-field tricritical to the classical mean-field behavior.

The impact of aerosils is much stronger compared to the recently published results on the Sm-A–Sm-C transition of $\bar{8}S5$ [25], where a crossover from mean-field tricritical to classical mean field (steplike evolution of C_p) was observed. In that case, even for concentrations higher than the ones measured here, the trace of the Sm-A–Sm-C transition is clearly observable. Both x-ray and calorimetric results suggest that the Sm-A–Sm-C* transition of chiral LCs is more susceptible to the aerosil-induced disorder, in contrast with the Sm-A–Sm-C transition of nonchiral compounds, which retains bulklike features even for high aerosil concentrations [23,25].

Similar heat capacity results were observed in the case of the hydrophobic aerosils (Fig. 6) with slightly less pronounced smearing compared to the case of hydrophilic aerosils. Variations on the enthalpies, transition temperatures, as well as the magnitude of the C_p jump are shown in Fig. 7.

In order to check the influence of aerosils on other polar and nonpolar compounds, the same set of experiments was performed on DOBAMBC and $\bar{8}S5$ hydrophobic aerosil

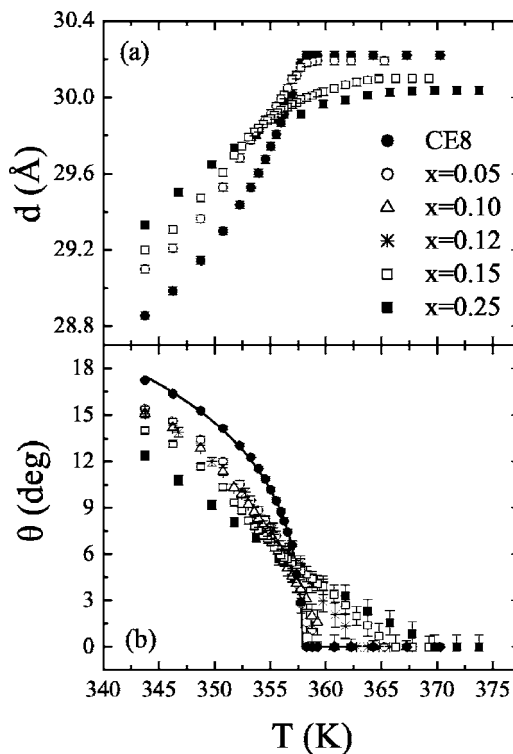


FIG. 3. (a) The smectic layer thickness (d) as a function of temperature (for clarity only selected data sets are shown) for CE8 and hydrophilic aerosil 300. (b) The tilt angle (θ) vs temperature is shown for CE8 bulk (solid circles), $x=0.05$ (open circles), $x=0.10$ (open triangles), $x=0.12$ (stars), $x=0.15$ (open squares), and $x=0.25$ (solid squares). The solid line represents the fit of bulk CE8 data using the extended mean-field ansatz.

mixtures. DOBAMBC is more polar but less chiral than CE8. Furthermore, it lacks N phase, i.e., the Sm-A phase melts directly to the I phase. In contrast, $\bar{8}S5$ is nonchiral and is less polar than CE8 and DOBAMBC. In Fig. 8(a), a wide range x-ray intensity versus wave vector q is shown for

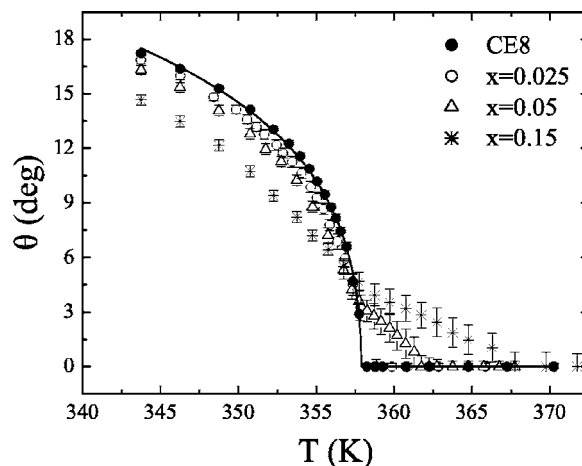


FIG. 4. The tilt angle (θ) vs temperature for bulk CE8 (solid circles) and hydrophobic aerosil mixtures $x=0.025$ (open circles), $x=0.05$ (open triangles), and $x=0.15$ (stars). The solid line is a fit of CE8 bulk data using an extended mean-field ansatz.

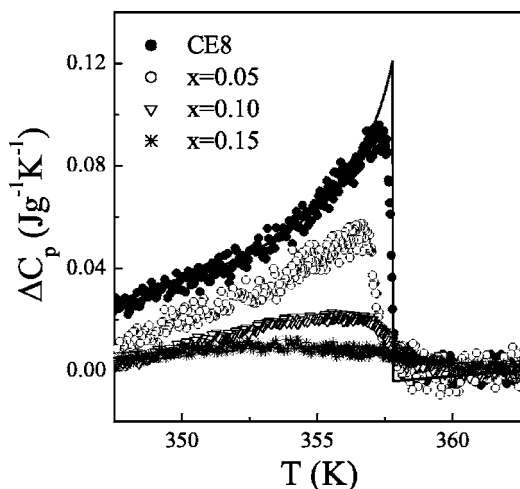


FIG. 5. Heat capacity (C_p) peak vs temperature for bulk CE8 (solid circles) and hydrophilic mixtures $x=0.05$ (open circles), $x=0.10$ (open triangles), and $x=0.15$ (stars). The solid line is a fit of CE8 bulk data using an extended mean-field ansatz.

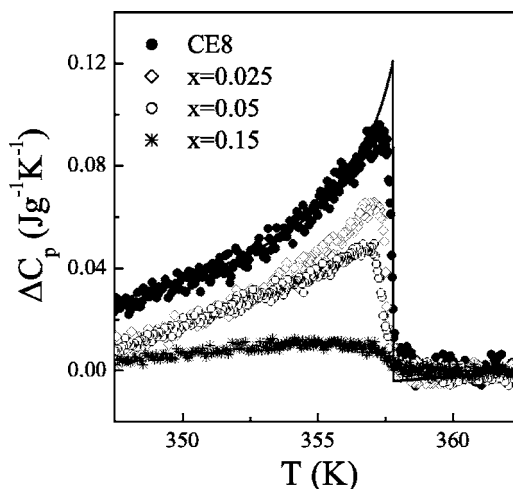


FIG. 6. Heat capacity (C_p) peak vs temperature for bulk CE8 (solid circles) and hydrophobic mixtures $x=0.025$ (open rhombus), $x=0.05$ (open circles), and $x=0.15$ (stars). The solid line is a fit of CE8 bulk data using an extended mean-field ansatz.

DOBAMBC bulk and two hydrophobic aerosil mixtures. Similar to what was found for CE8, the significant change of the background intensity is observed with increasing x , and clear first- and second-harmonic quasi-Bragg smectic peaks appear at higher values of q . The smectic peaks are becoming more broadened with increasing x [Figure 8(b)], as in the case of CE8.

Pretransitional behavior of the tilt angle is also recorded in the case of DOBAMBC+aerosil mixtures, though it is less pronounced than for CE8. The tilt angle data of small concentrations ($x=0.03$ and 0.08) can be nicely scaled to those of bulk (Fig. 9) if plotted versus $T-T_c$, apart from a small temperature range near T_c where a pretransitional behavior was observed. This behavior becomes pronounced at higher x values ($x=0.15$ and 0.25). The influence of disorder is milder compared to CE8, but still more intense than for $\bar{8}S5$ [23]. In contrast to CE8, the transition temperature shift is considerably bigger in the case of DOBAMBC. For CE8, only a slight T_c shift (smaller than 1 K) increasing monotonically with x was observed, while in DOBAMBC the temperature shifts are exceeding the 10 K for higher concentra-

tions. The T_c shift in DOBAMBC is plotted in Fig. 10.

The situation is different in the case of $\bar{8}S5$. Mixtures of this compound with hydrophilic aerosils were studied in detail by means of x-ray scattering [23] and calorimetry [25]. In order to make a direct comparison with the chiral compounds CE8 and DOBAMBC, one mixture of $\bar{8}S5$ with hydrophobic aerosils was studied here ($x=0.15$) by x-ray scattering. In agreement to what was previously reported for the hydrophilic mixtures [23], a shift of about 3 K occurs for the transition temperature in the case of $x=0.15$, while the scattering profiles retain sufficient bulklike features (contrary to the respective hydrophobic mixtures of CE8 and DOBAMBC). In Fig. 11, the smectic layer thickness versus $T-T_c$ is shown for bulk $\bar{8}S5$ and aerosil mixture of $x=0.15$. Much smaller compression of smectic layers is observed here (Fig. 12) than in the case of CE8 and DOBAMBC. Figure 12

TABLE I. The fitting parameters b/c in rad^2 as defined in [47] and T_c obtained from x-ray data of CE8 and DOBAMBC.

Sample	x	b/c	T_c (K)
CE8	0	0.088	357.88
CE8+aerosil 300	0.05	0.134	357.50
CE8+aerosil 300	0.10	0.144	357.25
CE8+aerosil R812	0.025	0.155	357.86
CE8+aerosil R812	0.05	0.229	357.84
DOBAMBC	0	0.016	366.45
DOBAMBC+aerosil R812	0.03	0.091	357.99
DOBAMBC+aerosil R812	0.08	0.105	356.35
DOBAMBC+aerosil R812	0.15	0.131	354.20

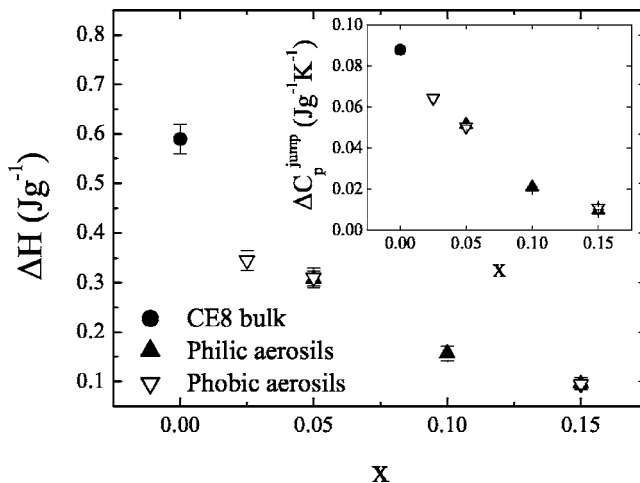


FIG. 7. The enthalpy of the Sm-A to Sm-C* phase transition for bulk CE8 (solid circles), hydrophilic (solid triangles), and hydrophobic mixtures (open triangles). In the inset, the magnitude of the C_p jump at T_c is shown.

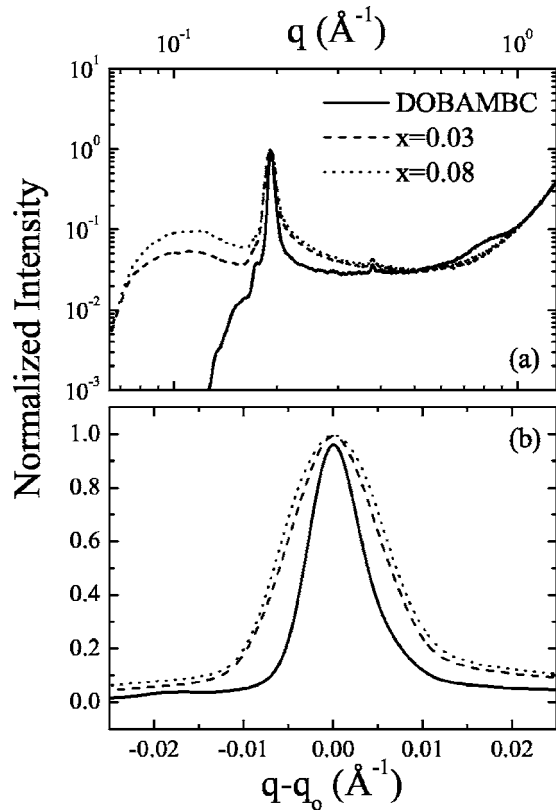


FIG. 8. (a) A wide-range x-ray spectrum of normalized intensity vs the wave vector q for bulk DOBAMBC (solid line) and two hydrophobic aerosil mixtures $x=0.03$ (dashed line) and $x=0.15$ (dotted line) is shown. (b) The first harmonic peak for all samples is plotted versus $q - q_0$.

shows the reduced compression of layers $(d_o - d)/d_o$ deep in the Sm-A phase for all CE8, DOBAMBC, and 8S5 mixtures.

V. THEORETICAL ANALYSIS

In this section, we present different mechanisms likely contributing to the observed behavior. We first estimate the condition under which the aerosil concentration is high enough to trigger global structural change upon the LC ordering. We then discuss different possible mechanisms giving rise to the measured smectic layer shrinkage.

A. Aerosil-induced global orientational deformation

We estimate the condition where a global LC elastic deformation is expected due to the presence of aerosil particles in the nematic and smectic-A phase. For this purpose, we compare the free energies of the system with (i) homogeneous and (ii) distorted LC ordering.

In case (i) we assume that the system's ordering is negligibly influenced by the aerosil particles. The resulting free energy of the system is then approximately $F_{\text{hom}} \sim A_i W$. In this case, all significant free-energy costs arise from the misalignment at the LC-aerosil interface. The subscript "hom" labels homogeneous structure with negligible pretilt. The quantity $A_i \sim N4\pi R^2$ estimates the surface area of the LC-

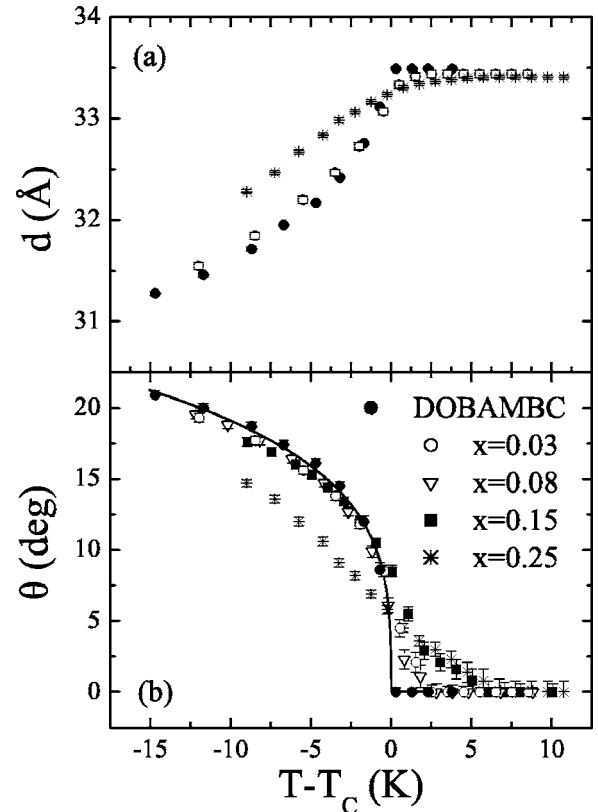


FIG. 9. (a) The smectic layer thickness (d) of bulk DOBAMBC and hydrophobic aerosil mixtures is plotted as a function of $T - T_c$ (for clarity, only selected data sets are shown). (b) The tilt angle (θ) vs $T - T_c$ is shown for bulk DOBAMBC (solid circles), $x=0.03$ (open circles), $x=0.08$ (open triangles), $x=0.15$ (solid squares), and $x=0.25$ (stars) mixtures. The solid line represents the fit of bulk DOBAMBC data using the extended mean-field ansatz.

aerosil aggregate interface, where N stands for the number of aerosil aggregates.

In the competing distorted configuration, the conditions at the aerosil-LC interface are strictly obeyed. Consequently,

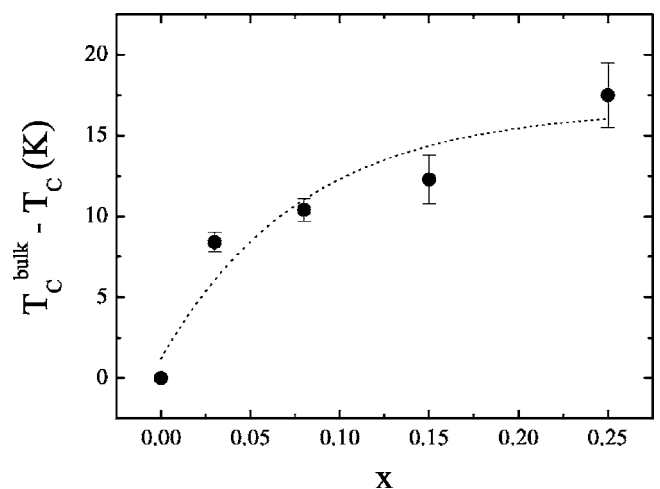


FIG. 10. The shift of T_c vs concentration x for the various hydrophobic aerosil dispersions in DOBAMBC. The dotted line is a guide to the eye.

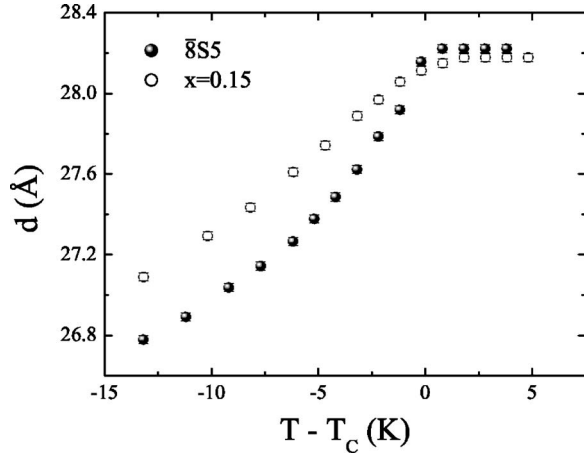


FIG. 11. The smectic layer thickness vs $T-T_c$ for $\bar{8}S5$ and hydrophobic aerosil mixture of $x=0.15$.

the anchoring contribution is negligible. However, this triggers elastic distortions in the remaining volume occupied by LC molecules. In a volume l_0^3 the elastic free-energy density penalty in the orientational ordering is approximately given by K/l_0^2 . Here we have assumed that a typical elastic orientational distortion evolves over the material-characteristic length l_0 of the sample. In the smectic-*A* phase, we roughly estimate the smectic elastic free-energy density due to the deviation of LC molecules from the smectic layer normal by $C_\perp \eta^2 q_0^2 \langle \theta^2 \rangle$. Here the smectic part of the free energy density is expanded up to second order in the tilt angle θ and $\langle \dots \rangle$ stands for the spatial average. It follows $F_{dis} \sim N(Kl_0 + C_\perp \eta^2 q_0^2 \langle \theta^2 \rangle l_0^3)$, where the subscript “dis” labels the distorted structure in which a global pretilt θ_t can be expected in the Sm-*A* phase.

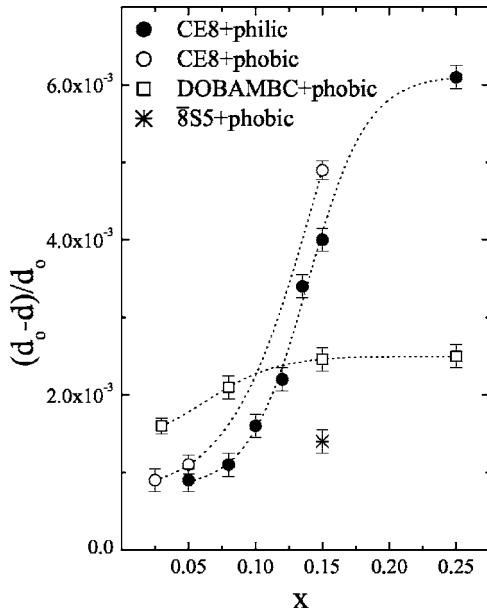


FIG. 12. The reduced compression of layers for CE8 and hydrophilic/hydrophobic mixtures (solid/open circles), DOBAMBC and hydrophobic mixtures (open squares), and $\bar{8}S5$ and hydrophobic aerosil mixtures (stars).

The tradeoff between these two estimates defines the threshold condition separating regimes with negligible and finite pretilt value. The configuration with global elastic deformation is expected when $F_{hom}/F_{dis} \sim \frac{4\pi R^2 W}{Kl_0 + C_\perp \eta^2 q_0^2 \langle \theta^2 \rangle l_0^3} = \frac{4\pi R^2}{d_e l_0 (1 + \langle \theta^2 \rangle l_0^2 / \lambda_\perp^2)} > 1$. Taking into account $l_0 \sim 2/(\rho_a a) \sim 2/(x\rho_{LC}a)$, the distorted phase is realized provided $x > x_t$. In the nematic phase (i.e., $\eta=0$), it follows that

$$x_t \equiv \frac{d_e}{2\pi R^2 a \rho_{LC}}. \quad (15)$$

Setting $K \sim 5 \times 10^{-12}$ J/m, $a \sim 300$ m²/g, $R = n_a \times 3.5$ nm, $n_a \sim 3$, $W \sim w_a 10^{-4}$ J/m², and $\rho_{LC} \sim 1$ g/cm³, we obtain the threshold condition $x_t \sim 0.1$ for $w_a = 2$. Here the estimate for n_a is obtained from our x-ray data.

In the smectic phase, the value of x_t is increased due to the presence of additional elastic distortions in the translational degree of freedom. In the case in which the smectic contribution is prevailing, we obtain

$$x_t \equiv \left(\frac{2d_e \langle \theta^2 \rangle}{\pi R^2 \lambda_\perp^2} \right)^{1/3} \frac{1}{a \rho_{LC}}. \quad (16)$$

For the set of the above-listed material parameters and $\lambda_\perp \sim 5$ nm, $\sqrt{\langle \theta^2 \rangle} \sim 3^\circ$ it follows that $x_t \sim 0.15$.

In the following two subsections, we assume that the aerosil particles enforce a finite pretilt θ_t at the LC-aerosil interface. It reflects the compromise between local orientational elastic and surface anchoring penalties. In the Sm-*A* phase, θ_t can give rise to shrinkage of smectic layers. In addition, it can cause an inhomogeneous θ profile. We study separately both of these phenomena below. In reality, a combination of both effects takes place.

B. Pretilt driven smectic layer compression

We now set that the aerosil-induced pretilt $\theta = \theta_t$ is enforced at the LC-aerosil interface in the Sm-*A* phase. Due to geometrical constraints, the pretilt tends to shrink the smectic layers.

To estimate the average compression of layers, we assume that the LC experiences a spatially uniform tilt. For a relatively small value of θ , we expand the free-energy density up to the quartic term in θ . After the integration over the volume V_{LC} occupied by the LC phase, we obtain [see Eq. (3)]

$$F \sim (atq^2\theta^2 + bq^4\theta^4)V_{LC} + A_i W(\theta_t - \theta)^2/2. \quad (17)$$

We refer to the volume and interface parts in Eq. (17) as the *inherent* and *external* contribution, respectively. The *inherent* contribution, weighted by V_{LC} , tends to impose the elastically favored ordering. This is embodied in the following expressions for the tilt angle: $\theta(T > T_c) = 0$ and $\theta(T < T_c) \sim \sqrt{\frac{aT}{2bq_0^2}}$. On the other hand, the *external* contribution due to the aerosil particles enforces $\theta = \theta_t$, where A_i estimates the overall LC-aerosil interface.

In the Sm-*A* phase, the two contributions result in the establishment of a global finite pretilt. From $\frac{\partial F}{\partial \theta} = 0$, we get $\theta \sim \theta_t / (1 + \frac{2\alpha V_{LC}}{WA_i})$, where $\alpha = atq^2$. For relatively low concen-

trations ρ_a and taking into account Eq. (14), it follows that

$$\frac{\theta}{\theta_t} \sim \frac{\rho_a W}{\rho_s \alpha R} \sim x \frac{\rho_{LC} \xi^2}{\rho_s R d_e}. \quad (18)$$

For $d=d_0 \cos \theta \sim d_0(1-\theta^2/2)$, we obtain

$$\Delta d \sim \frac{\theta_t^2 x^2}{2} \left(\frac{\rho_{LC} \xi^2}{\rho_s R d_e} \right)^2. \quad (19)$$

C. Global average tilt without smectic layer compression

We next neglect the layer shrinkage and estimate the influence of θ_t on the average tilt $\langle \theta \rangle$ in the Sm-A phase. We assume that θ_t temperature dependence is relatively weak in comparison to the bulk $\theta(T)$ response across the Sm-A–Sm-C transition. This interface-induced distortion persists over distances that are roughly equal to the “effective” smectic penetration length,

$$\lambda_{\text{eff}} = \sqrt{\frac{1}{\frac{1}{\lambda^2} + \frac{1}{\xi_D^2}}}. \quad (20)$$

Here $\lambda = \frac{\lambda_0}{\sqrt{f_{\text{eff}}}}$ [see Eq. (11)] stands for the average bulk smectic penetration length and t_{eff} is the effective reduced temperature (see Sec. V D). The bare average penetration length λ_0 is comparable to the typical molecular length of the system and we set $C \sim C_{II} \sim C_{\perp}^{(0)} T_c$. Note that λ_{eff} does not diverge at the pseudo-phase-transition realized at $t_{\text{eff}}=0$, because its value is limited by finite-size effects. We describe the upper bound by ξ_D , i.e., $\lambda_{\text{eff}}(t_{\text{eff}}=0) = \xi_D$. In our calculations we set $\xi_D \sim l_0$. We henceforth refer to the volume V_t in which LC molecules are apparently perturbed by aerosil particles as the aerosil coherence volume.

We estimate an average tilt angle $\langle \theta \rangle$ of the sample by

$$\langle \theta \rangle \sim \frac{\theta_t V_t + \theta V_b}{V_{LC}}. \quad (21)$$

The bulk tilt $\theta(T)$ dependence is given by Eq. (7).

The quantity V_b refers to the volume occupied by LC molecules with bulklike local ordering and the quantity $V_{LC} = V_b + V_t$ to the volume of all LC molecules. Therefore, V_t refers to the volume occupied by essentially tilted LC molecules. In estimating the values of volumes entering the expression for $\langle \theta \rangle$, we consider two different cases. In the first case, the aerosil unit is a spherular aerosil particle or spherular cloud of them of radius R , which are roughly homogeneously distributed. In the second case, the aerosil unit locally resembles a linelike object of average length l . In both cases, the average separation between units is given by l_0 . We refer to these two examples as the *point* and *line* cases. The corresponding volumes per aerosil unit are then expressed as

$$V_t^{(\text{point})} \sim \frac{4\pi}{3} [(R + \lambda_{\text{eff}})^3 - R^3],$$

$$V_{LC}^{(\text{point})} \sim \frac{4\pi}{3} [(R + l_0)^3 - R^3],$$

$$V_t^{(\text{line})} \sim \pi l [(R + \lambda_{\text{eff}})^2 - R^2],$$

$$V_{LC}^{(\text{line})} \sim \pi l [(R + l_0)^2 - R^2],$$

and we approximately set $1/(\lambda_{\text{eff}})^2 \sim |(T_c - T)/T_c|/\lambda_0^2 + 1/l_0^2$. At $T \sim T_c$, our expressions yield $V_{LC}^{(\text{case})} \sim V_t^{(\text{case})}$. However, this description underestimates the density of aerosil particles. For this reason, we weigh the ratio $V_t^{(\text{case})}/V_{LC}^{(\text{case})}$ with the factor w . In the corrected ratio $\kappa = w V_t^{(\text{case})}/V_{LC}^{(\text{case})}$, we define w from the condition $\kappa(\lambda_{\text{eff}} \leq l_0/2) \equiv 1$. Therefore, if pairs of neighboring aerosil particles are separated on average by a distance, which is less than or equal to $2\lambda_{\text{eff}}$ then the whole LC body is significantly affected by θ_t . For such cases, we set $V_t = V_{LC}$. Consequently $w = [(R + l_0)^{n_{\text{case}}} - R^{n_{\text{case}}}] / [(R + \frac{l_0}{2})^{n_{\text{case}}} - R^{n_{\text{case}}}]$ and

$$\langle \theta \rangle^{(\text{case})}(T) \sim \theta(T) + [\theta_t - \theta(T)]\kappa, \quad (22)$$

$$\kappa = \frac{[(R + \lambda_{\text{eff}})^{n_{\text{case}}} - R^{n_{\text{case}}}]}{\left[\left(R + \frac{l_0}{2} \right)^{n_{\text{case}}} - R^{n_{\text{case}}} \right]}. \quad (23)$$

D. Distribution of phase transition temperatures

We analyze the influence of a distribution of Sm-A–Sm-C (pseudo) phase transition temperatures upon the temperature dependence of the tilt angle. We assume that the inhomogeneous aerosil spatial distribution reflects upon inhomogeneously distributed smectic layer strain [21]. Further, we take into account that elastic distortions in θ are also spatially dependent. These effects give rise to a spatial distribution of effective local phase transition temperatures.

We first study the influence of layer shrinkage $\Delta d = d_0 - d$ on the pseudo phase transition temperature $T_c^{(d)}$ for homogenous θ -profile. For this purpose, we expand f_v [see Eq. (3)] up to the quadratic term in θ . One obtains $\Delta f \equiv f_v - \eta^2 C_{II} (q - q_0)^2 = \eta^2 C_{\perp} q^2 \theta^2 - \eta^2 C_{II} q (q - q_0) \theta^2$, i.e.,

$$\Delta f = \eta^2 C_{\perp}^{(0)} (T - T_c^{(d)}) q^2 \theta^2. \quad (24)$$

The effective pseudo Sm-A–Sm-C phase transition temperature is expressed as

$$\frac{T_c^{(d)}}{T_c} = 1 + \frac{\Delta d}{d_0} \frac{C_{II}}{C_{\perp}^{(0)} T_c}. \quad (25)$$

Contrary to the N -Sm-A phase transition [45], the temperature shift of the Sm-A–Sm-C transition is sensitive to the sign of Δd . For dilated ($\Delta d < 0$) and compressed ($\Delta d > 0$) layers, the latter, transition temperature is either decreased or increased, respectively.

Temperature shifts can also be due to nonhomogeneous θ profiles. Namely, the gradient elastic contribution $|\nabla \theta|^2$ is proportional to $1/\lambda_{\text{eff}}^2$ [49], which could be spatially dependent.

We further assume that the transition temperatures are continuously distributed about an average transition temperature $\langle T_c^{(d)} \rangle$. This is due to local variations in the values of the smectic layer spacing as well as in the values of λ_{eff} .

We approximate the $T_c^{(d)}$ distribution $P(T_c^{(d)})$ with the Gaussian one,

$$P(T_c^{(d)}) = \frac{2}{\sigma\sqrt{\pi}} e^{-(T_c^{(d)} - \langle T_c^{(d)} \rangle)^2 / \sigma^2}, \quad (26)$$

$$\sigma = \frac{\Delta T}{2 \ln 2}, \quad (27)$$

where ΔT describes the half-width at half-height of the distribution. We calculate the resulting average tilt temperature dependence as

$$\langle \theta \rangle(T) = \int P(T_c^{(d)}) \theta(T, T_c^{(d)}) dT_c^{(d)}, \quad (28)$$

and $\theta(T, T_c^{(d)})$ is given by Eq. (7), where $t \equiv t_{\text{eff}} = (T - T_c^{(d)}) / T_c^{(d)}$ now stands for the effective reduced temperature.

E. Volume depletion and smectic layer compression

We next estimate the effect of volume depletion upon the layer shrinkage in the Sm-A phase. We set that the system volume V is constant, i.e., independent of x . Therefore, added aerosil particles reduce the volume available to LC molecules. In this estimate, we consider the system that is enclosed within a cube of volume $V=L^3$. We assume that in the pure Sm-A phase, the layers are unconstrained and periodically stacked along one cube length. Therefore $L=N_d d_0$, where N_d stands for the number of smectic layers along this direction. When aerosil particles are added, the volume available to LC phase reduces to $V_{\text{LC}}=L^3 - N_a \frac{4\pi R^3}{3}$. Taking into account Eq. (14), we obtain $V_{\text{LC}}=L^3(1 - \rho_a/\rho_s)=L^2 N_d d$. If the number of smectic layers is conserved, then $V_{\text{LC}}/V=d/d_0$, yielding

$$\frac{\Delta d}{d_0} \sim \frac{\rho_a}{\rho_s} \sim \frac{\rho_{\text{LC}}}{\rho_s} x. \quad (29)$$

Note that our experiments were carried out under a constant pressure. Consequently, an alternative scenario is also possible in which the reduced volume available for the LC simply reduces the amount of LC phase in the volume with a subsequent reduction of the number of smectic layers with no compression. Therefore the obtained expression for the layer shrinkage represents an upper limit estimate.

F. Interaction between aerosil particles

We analyze how long-range interactions between aerosil particles could influence the extent of layer shrinkage in the Sm-A phase. These interactions mainly arise from topological reasons and are dominantly mediated by an intervening nematic director field.

To demonstrate this effect, we consider two aerosil particles. For strong anchoring each of them is equivalent to a radial hedgehog defect. The latter condition is realized for $WR/K=R/d_e > 1$. By setting $K \sim 5 \times 10^{-12}$ N and $R=R_a=3.5$ nm, this condition is fulfilled for $W > 10^{-3}$ J/m². If an aerosil unit is made of several particles, that decreases the threshold value of W , above which a strong anchoring regime is roughly imposed to surrounding LC molecules. The radial defect in the orientational order bears the topological charge of strength one.

If an aerosil particle plays the role of a radial hedgehog defect, it triggers the formation of a neighboring hyperbolic defect [50]. The sum of topological charges of both defects is zero, enabling preferentially homogeneous alignment relatively far from such a pair of defects. The defects attract each other, but cannot annihilate [51], because the radial director field surrounding the aerosil particle is not equivalent to a real nematic defect for relatively small separations (with respect to the nematic correlation length) of interacting defects. Consequently, a topological dipole is formed, which in the nematic phase is surrounded by the director field in a fashion similar to the electric field of an electric dipole [52]. Note that it was shown that in case of colloidal particles immersed in a nematic LC phase, the electrostatic analogy works surprisingly well, at least for predicted spatial scaling relations [52].

By adopting the scenario described above, a network of interacting topological dipoles can be formed in the LC-aerosil mixture. Let us assume that the neighboring dipoles are separated in the Sm-A phase by smectic layers and that the interaction between them on average compresses the layers. By increasing x , the average distance between dipoles decreases, yielding a stronger interaction and consequently a larger layer compression.

In order to estimate the average layer compression, we express the long-range interaction energy between two topological defects. In the lowest order approximation, it is equal to

$$U_{\text{dip}} \sim 8\sigma\pi K R_a^4 / r^3 \quad (30)$$

(for a pair of dipoles separated by the distance r that are aligned along the same direction [50]). The constant σ is of the order of 1. An average compression free-energy density f_{com} roughly equals

$$f_{\text{com}} \sim C_{II} \eta^2 (q - q_0)^2 \sim C_{II} \eta^2 q_0^2 (\Delta d / d_0)^2. \quad (31)$$

In the diluted regime (i.e., $x \ll 1$), there is on average one dipole per volume $V \sim l_0^3$. By setting $f_{\text{com}} l_0^3 \sim U_{\text{dip}}$ and $r \sim l_0$, one gets the estimate

$$\frac{\Delta d}{d_0} \sim \sqrt{\frac{8\sigma\pi K R_a^2}{\eta^2 C_{II} q_0^2 l_0^3}} \sim \sqrt{8\sigma\pi} \frac{\lambda_{II} R_a^2}{l_0^3}. \quad (32)$$

Deep in the Sm-A phase, λ_{II} is comparable to a typical molecular size. By setting $\lambda_{II}=d_0$, one gets

$$\frac{\Delta d}{d_0} \sim \sqrt{8\sigma\pi} \frac{d_0 R_a^2}{l_0^3} \sim \sqrt{\frac{\sigma\pi}{8}} d_0 R_a^2 a^3 \rho_{\text{LC}}^3 x^3. \quad (33)$$

In the Sm-A phase, however, the strong influence of the smectic layers on the director field screens the dipole-dipole interaction, thus reducing the magnitude of layer compression due to long-range aerosil interactions. We next show, that this influence is relatively strong and that the presence of smectic layers plays a role similar to external electric or magnetic field.

For simplicity, we consider a planar case, where the director is confined within the (x, z) plane. We parametrize it as $\vec{n}=(\sin \theta, 0, \cos \theta)$. The external homogeneous electric or magnetic field is aligned along the z axis. In the nematic phase, the corresponding free-energy density reads $f=K/2(|\nabla\theta|^2-\cos^2\theta/\xi_f^2)$, where ξ_f stands for the external field coherence length [46]. For relatively small θ values, realized in a relatively strong field, it follows that

$$f \sim \frac{K}{2} \left(|\nabla\theta|^2 + \frac{\theta^2}{\xi_f^2} \right) + f_0. \quad (34)$$

Here $f_0=K/2\xi_f^2$ is independent of θ . We next consider planar director ordering in the Sm-A phase, where the smectic layers are homogeneously stacked along the z axis, i.e., $\phi=q_0z$. For relatively small deviations of \vec{n} from the z axis, we obtain

$$f \sim \frac{K}{2} \left(|\nabla\theta|^2 + \frac{\theta^2}{\lambda_\perp^2} \right). \quad (35)$$

By comparing Eq. (34) and Eq. (35), we conclude that the smectic ordering has a similar influence on \vec{n} as an external field, the strength of which is given by $\xi_f \sim \lambda_\perp$. Deep in the Sm-A phase, $\lambda_\perp \sim \text{nm} < l_0$, which corresponds to a relatively strong external field. Such a strong external field, for positive LC field anisotropy, aligns \vec{n} along its direction. Consequently, it screens the influence of a source that enforces inhomogeneous \vec{n} .

Note further that it is also possible that the topologically driven interaction between aerosil strands simply reduces the amount of LC between them, with a subsequent reduction of the number of essentially noncompressed smectic layers. Therefore, the expression (33) represents the upper limit estimate.

VI. DISCUSSION

We first comment that so far most studies suggest that the aerosil-induced disorder destroys quasi-long-range smectic order [1,16]. Therefore, the LC systems of interest are expected to exhibit short-range order. However, the temperature behavior of the heat capacity near the bulk Sm-A–Sm-C phase transition temperature exhibits a pronounced anomaly, particularly for $x < 0.1$. Already a few studies contradict these conclusions [53,54]. Consequently, we henceforth refer to the observed anomalous responses in our samples as *phase transitions*, although in reality they might not correspond to a true thermodynamic phase transition.

The x-ray intensity profiles $I(q)$, shown in Figs. 2 and 8, yield information on the temperature dependence of the average smectic layer spacing d . In particular, the $I(q)$ profiles

reveal temperature-driven structural changes in the aerosil network. From the layer spacing measurements obtained as T and x is varied, the average smectic tilt angle θ can be calculated based on the following assumptions: The layer shrinkage $\Delta d = d_0 - d = \Delta d^{(t)} + \Delta d^{(o)}$ at an arbitrary temperature originates either from the tilt of LC molecules from the smectic layer normal (the $\Delta d^{(t)}$ term) or from other mechanisms (the $\Delta d^{(o)}$ contribution). The $\Delta d^{(o)}$ shrinkage arises predominantly due to the aerosil-driven volume depletion (see Sec. V E). Moreover, we predict that below T_c , the $\Delta d(T)$ variation is dominated by $\Delta d^{(t)}$ temperature changes. We estimate the $\Delta d^{(o)}$ value as $\Delta d^{(o)} \sim d_0 - d(T)$, where $T \sim T_c + 5$ K corresponds to a temperature deep in the Sm-A phase. Thus we set that at these temperatures the smectic layers are compressed on average due to the mechanisms that do not involve tilting of LC molecules. This prediction is justified at least in the soft regime. Consequently, we calculate the $\theta(T)$ dependence via the relation [see Eq. (5)]

$$\Delta d^{(t)}(T) = (d_0 - d + \Delta d^{(o)}) \cos \theta. \quad (36)$$

The $\theta(T)$ data are shown in Figs. 3, 4, and 9. They reveal qualitatively similar LC structural changes on varying x in both hydrophilic and hydrophobic samples and for all LCs. In the following, we discuss possible origins of the observed behavior.

The key assumption is that due to geometrical reasons, the aerosil particles give rise to tilting of the LC molecules with respect to the smectic layer normal even above T_c . In this picture, the aerosil particles can be visualized as forming short elongated strands, while the smectic layers intervene between the neighboring strands. On average, the layer normal is roughly parallel to these strands. In such a case, the homeotropic anchoring at the LC-aerosil interface enforces on average a tilt to the LC molecules. We henceforth refer to the aerosil enforced tilt as the pretilt angle θ_t , which reflects the compromise between the anchoring tendency and LC elastic penalties. Note that it is also possible that the smectic layer normal is perpendicular to the strand, i.e., the layers are stacked between the neighboring strands. In this case, either dilatation (that is not observed) or compression of smectic layers due to volume depletion is expected. In Sec. V A, we estimate the critical concentration x_t of the aerosils, for which a global structural change is expected in the LC orientational ordering. The rough estimate suggests that for common LC materials, these changes are anticipated for $x > 0$. Therefore, Eq. (36) works well for $x < x_t$. If the pretilt is the dominant contribution in the observed behavior, two qualitatively different responses of the smectic ordering can be expected. For the first one, we assume that θ_t enforces an apparent tilt of the LC molecules over the distance given by the smectic penetration length as analyzed in Sec. V C. The second possible response gives rise to a global tilting of the LC molecules due to the pinning of smectic layer thickness [45].

We considered the pretransitional phenomena above the pseudo Sm-A–Sm-C phase transition temperature. Some representative fits of experimental data, using different assumptions, are shown in Fig. 13. For $x \lesssim 0.05$, the measurements could be roughly reproduced solely by introducing a

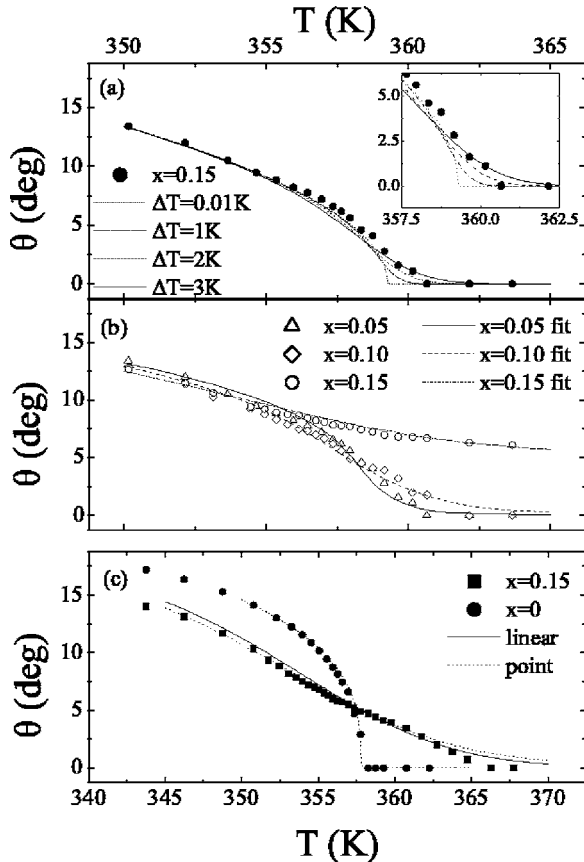


FIG. 13. The tilt temperature variation for different concentrations x . Symbols mark measurements (CE8) and lines represent theoretical predictions. In (a) we take into account only different widths of the distribution Eq. (26), $\theta_i=0$. In (b) and (c), we allow a finite pretilt and assume that the aerosil-induced tilt persists over the effective smectic penetration length [see Eq. (22)]. (b) $\Delta d^{(o)}=0$; $x=0.05$, $\lambda_0=1.2$ nm, $\theta_i=1.7^\circ$, $\Delta T=1$ K; $x=0.10$, $\lambda_0=0.9$ nm, $\theta_i=2.8^\circ$, $\Delta T=3$ K; $x=0.15$, $\lambda_0=2.4$ nm, $\theta_i=9.8^\circ$, $\Delta T=6$ K. (c) In fitting the $x=0.15$ case, the full line and dotted line correspond to the “line” and “point” version of the model described in Sec. V C. Model parameters are $\theta_i=5^\circ$, $\Delta T=5$ K, $\lambda_0=1$ nm, and $\Delta d^{(o)} \sim d_0 - d(T_{\text{deep}})$, where T_{deep} corresponds to the temperature deep in the Sm-A phase.

distribution [Fig. 13(a) and Eq. (27)] of domain transition temperatures and setting $\theta_i=0$. For $x \geq 0.05$, it was necessary to allow for a finite value of θ_i in order to get reasonable qualitative and quantitative agreement between experiment and theory. In Fig. 13(b), we set that the behavior is dominated by the tilt of LC molecules [i.e., we put $\Delta d^{(o)}=0$ and use Eq. (6)], while in Fig. 13(c) we use Eq. (36).

In order to qualitatively reproduce the change in $\Delta d(x)$ behavior in the Sm-A phase, as x is varied, we had to invoke into the model pretilt enforced global tilting of LC molecules (Sec. V B). In this scenario, the average tilt depends on the relative strength of the bulk Sm-A elastic and the surface anchoring orientation free-energy contribution. The bulk term, favoring $\theta=0$, prevails for $x \ll 0.1$. For large enough values of x , the anchoring term, enforcing $\theta=\theta_i$, becomes dominant. A crossover between the two regimes takes place at $x \sim 0.1$, which coincides with the intermediate-rigid aerosil

network structural transition. Note that this structural transition makes the response of d as x is varied stronger as anticipated by Eq. (19). The reason behind it is the lost ability of the aerosil network to reduce elastic deformations in a LC phase by local restructuring of the aerosil network.

There exist various possible mechanisms giving rise to the smectic layer compression $\Delta d^{(o)}$, which exclude tilt of LC molecules. It could be either due to the reduced volume available to the Sm-A or due to the addition of aerosil particles. Our experiments were carried out under constant pressure. Therefore, the analysis in Sec. V E estimates the maximal possible layer shrinkage due to this effect, suggesting $\Delta d \propto x$. In Sec. V F, we further analyze how interactions among aerosil particles could influence the layer compression. These interactions arise mainly due to topological reasons [50]. We show that the presence of smectic layers strongly depresses these interactions, making this source of layer shrinkage negligible well above T_c .

We next comment on the influence of LC chirality on Δd . Our results indicate that with increasing chirality strength the layer shrinkage increases. This result might be due to geometrical constraints. In case that pretilt dominantly influences the tilt, one has in general contradicting tilting tendencies at the nearby strands, as discussed in this section. Consequently the molecules in between the strands tend to be pushed along the smectic layer normal. In chiral samples this frustration could be avoided by moving molecules along the smectic cone, which is energetically less costly [55].

We further discuss the heat capacity behavior at the (pseudo) Sm-A–Sm-C phase transition. In bulk samples the MF, tricritical-type behavior is observed. With increasing x the smeared steplike MF behavior is approached. This phenomenon could be observed by taking into account the results of Benguigui and Martinoty [56]. They show that the coupling between the Sm-C order parameter (the tilt angle θ) and the strains effectively renormalizes the coefficient in front of the fourth-order term in the θ expansion of the free energy [i.e., the coefficient b in Eq. (4)]. For strong enough coupling this coefficient vanishes, giving rise to the tricritical behavior. We claim that the aerosil particles, which introduce into the system a kind of random disorder, decrease the strength of this coupling. Therefore, the value of b with increasing x increases and the steplike MF behavior is approached.

We finally discuss the influence of x on the temperature shift of T_c for the pseudo Sm A–Sm-C phase transition. The temperature shift in a sample reveals mainly the interplay between the elastic and surface interactions. Recent results indicate that finite-size effects [2,42] might also be important. Note that the elastic contributions arise due to deformations in the orientational order and also due to the compression of the smectic layers, as is shown in Sec. V D. These sources tend to decrease and increase (for $\Delta d > 0$) T_c , respectively. Further, the surface contribution tends to increase T_c .

VII. CONCLUSIONS

We have studied experimentally and theoretically the influence of aerosils on phase behavior of various LCs (CE8,

DOBAMBC, and $\bar{8}S5$) in the Sm-A, nonchiral, and chiral Sm-C phases. We have systematically analyzed the impact of (i) aerosil concentration x , (ii) hydrophilic and hydrophobic spherular aerosils' surface tendency, and (iii) LC chirality on smectic structural details and on the Sm-A–Sm-C* phase transition.

In the experimental part of the work, we used x-ray scattering, which directly probes the average smectic layer thickness d and gives information on structural changes in the aerosil network. The Sm-A–Sm-C* phase transition anomalies have been investigated by means of high-resolution calorimetry. In order to explain qualitatively the experimental results, we used a Landau–de Gennes-Ginzburg-type phenomenological approach focusing on LC orientational and smectic layer phase translational degrees of freedom.

The following structural changes have been observed experimentally on increasing x . In all the samples, in the Sm-A phase, the smectic layer thickness at a given temperature decreases monotonically. The effect is comparable for hydrophobic and hydrophilic aerosils, but it is slightly more pronounced in the latter case. However, the layer shrinkage strongly decreases with reduced LC chirality. In chiral samples, on increasing x , the layer shrinkage exhibits a pronounced crossover behavior in the region where the soft-stiff transition of the aerosil network takes place. Furthermore, on increasing x in all samples (see also Ref. [24]) the Sm-A–Sm-C* phase transition gradually crosses from the tricritical mean field (MF) at $x \sim 0$ toward MF behavior realized in the high aerosil density regime ($x \leq 0.10$). The

phase transition temperature monotonically decreases with x in all samples, although the magnitude of the transition shifts is sample-dependent.

Our analysis suggests that the main reason behind layer shrinkage is the aerosil-induced tilt of LC molecules with respect to smectic layers. Taking this into account, we qualitatively and quantitatively reproduce the measured $d(x, T)$ profiles, provided that the spatial variation of the local effective temperature is also considered. We believe that the x driven crossover from the tricritical MF toward steplike MF behavior is due to weakened coupling between the smectic-C order parameter and the strain in the system. The main reason behind temperature shifts is elastic distortions, the strength of which monotonically increases with x .

Note that our analysis shows that experimental data could be qualitatively well reproduced taking into account the above described mechanisms. However, it might also be possible that suppression and the reduction of the LC fluctuation spectrum in the translational degree of ordering could also contribute to variations in d . Consequently the system becomes stiffer and this might induce reduced layer spacing.

ACKNOWLEDGMENTS

This research was supported by Slovenian Office of Science under the Program PO-0523, project J1-6593, ESF project COSLAB, and Slovenian-Greek bilateral cooperation project funded by the General Secretariat of Research and Technology of Greece.

-
- [1] T. Bellini, L. Radzihovsky, J. Toner, and N. A. Clark, *Science* **294**, 1074 (2001).
 - [2] G. S. Iannacchione, C. W. Garland, J. T. Mang, and T. P. Rieker, *Phys. Rev. E* **58**, 5966 (1998).
 - [3] T. Jin and D. Finotello, *Phys. Rev. E* **69**, 041704 (2004).
 - [4] M. Marinelli, F. Mercuri, S. Paoloni, and U. Zammit, *Phys. Rev. Lett.* **95**, 237801 (2005).
 - [5] G. Cordoyiannis, G. Nounesis, V. Bobnar, S. Kralj, and Z. Kutnjak, *Phys. Rev. Lett.* **94**, 027801 (2005).
 - [6] G. Sinha, J. Leys, C. Glorieux, and J. Thoen, *Phys. Rev. E* **72**, 051710 (2005).
 - [7] A. Barabasi and E. Bonabeau, *Sci. Am.* **288**, 50 (2003).
 - [8] J. Barré, A. R. Bishop, T. Lookman, and A. Saxena, *Phys. Rev. Lett.* **94**, 208701 (2005).
 - [9] B. Zhou, G. S. Iannacchione, C. W. Garland, and T. Bellini, *Phys. Rev. E* **55**, 2962 (1997).
 - [10] H. Haga and C. W. Garland, *Liq. Cryst.* **23**, 645 (1997).
 - [11] F. Mercuri, A. K. Ghosh, and M. Marinelli, *Phys. Rev. E* **60**, R6309 (1999).
 - [12] M. Marinelli, A. K. Ghosh, and F. Mercuri, *Phys. Rev. E* **63**, 061703 (2001).
 - [13] A. Hourri, T. K. Bose, and J. Thoen, *Phys. Rev. E* **63**, 051702 (2001).
 - [14] T. Jin and D. Finotello, *Phys. Rev. Lett.* **86**, 818 (2001).
 - [15] S. Park, R. L. Leheny, R. J. Birgeneau, J. L. Gallani, C. W. Garland, and G. S. Iannacchione, *Phys. Rev. E* **65**, 050703(R) (2002).
 - [16] R. L. Leheny, S. Park, R. J. Birgeneau, J. L. Gallani, C. W. Garland, and G. S. Iannacchione, *Phys. Rev. E* **67**, 011708 (2003).
 - [17] G. S. Iannacchione, S. Park, C. W. Garland, R. J. Birgeneau, and R. L. Leheny, *Phys. Rev. E* **67**, 011709 (2003).
 - [18] P. S. Clegg, C. Stock, R. J. Birgeneau, S. Park, C. W. Garland, G. S. Iannacchione, R. Leheny, and M. Neubert, *Phys. Rev. E* **68**, 021703 (2003).
 - [19] T. Bellini, N. A. Clark, V. Degiorgio, F. Mantegazza, and G. Natale, *Phys. Rev. E* **57**, 2996 (1998), and references therein.
 - [20] A. Roshi, G. S. Iannacchione, P. S. Clegg, and R. J. Birgeneau, *Phys. Rev. E* **69**, 031703 (2004).
 - [21] Z. Kutnjak, S. Kralj, and S. Žumer, *Phys. Rev. E* **66**, 041702 (2002).
 - [22] Z. Kutnjak, G. Cordoyiannis, and G. Nounesis, *Ferroelectrics* **294**, 105 (2003).
 - [23] P. S. Clegg, R. J. Birgeneau, S. Park, C. W. Garland, G. S. Iannacchione, R. L. Leheny, and M. E. Neubert, *Phys. Rev. E* **68**, 031706 (2003).
 - [24] D. Liang, M. A. Borthwick, and R. Leheny, *J. Phys.: Condens. Matter* **16**, S1989 (2004).
 - [25] A. Roshi, G. S. Iannacchione, P. S. Clegg, R. J. Birgeneau, and M. E. Neubert, *Phys. Rev. E* **72**, 051706 (2005).
 - [26] S. Róžański and J. Thoen, *Liq. Cryst.* **32**, 331 (2005).
 - [27] S. Róžański and J. Thoen, *Liq. Cryst.* **32**, 1013 (2005).

- [28] S. Rózański and J. Thoen, *J. Non-Cryst. Solids* **351**, 2802 (2005).
- [29] G. Cordoyiannis, S. Kralj, G. Nounesis, S. Žumer, and Z. Kutnjak, *Phys. Rev. E* **73**, 031707 (2006).
- [30] D. S. Fisher, G. M. Grinstein, and A. Khurana, *Phys. Today* **41**(12), 56 (1988).
- [31] Y. Imry and S. Ma, *Phys. Rev. Lett.* **35**, 1399 (1975).
- [32] A. Aharony and E. Pytte, *Phys. Rev. Lett.* **45**, 1583 (1980).
- [33] D. E. Feldman, *Phys. Rev. Lett.* **84**, 4886 (2000), and references therein.
- [34] T. Bellini, M. Buscaglia, C. Chiccoli, F. Mantegazza, P. Pasini, and C. Zannoni, *Phys. Rev. Lett.* **85**, 1008 (2000).
- [35] T. Bellini, M. Buscaglia, C. Chiccoli, F. Mantegazza, P. Pasini, and C. Zannoni, *Phys. Rev. Lett.* **88**, 245506 (2002).
- [36] P. A. Lebwohl and G. Lasher, *Phys. Rev. A* **6**, 426 (1972).
- [37] M. Caggioni, A. Roshi, S. Barjami, F. Mantegazza, G. S. Iannacchione, and T. Bellini, *Phys. Rev. Lett.* **93**, 127801 (2004).
- [38] F. Mercuri, S. Paoloni, U. Zammit, and M. Marinelli, *Phys. Rev. Lett.* **94**, 247801 (2005).
- [39] H. Haga and C. W. Garland, *Phys. Rev. E* **56**, 3044 (1997b).
- [40] C. W. Garland, *Thermochim. Acta* **88**, 127 (1985).
- [41] H. Yao, K. Ema, and C. W. Garland, *Rev. Sci. Instrum.* **69**, 172 (1998).
- [42] Z. Kutnjak, S. Kralj, G. Lahajnar, and S. Žumer, *Phys. Rev. E* **70**, 051703 (2004), and references therein.
- [43] R. B. Meyer, *Mol. Cryst. Liq. Cryst.* **40**, 33 (1977).
- [44] T. C. Lubensky and S. R. Renn, *Phys. Rev. A* **41**, 4392 (1990).
- [45] S. Kralj and T. J. Sluckin, *Phys. Rev. E* **50**, 2940 (1994).
- [46] P. G. de Gennes and J. Prost, *The Physics of Liquid Crystals* (Oxford University Press, Oxford, 1993).
- [47] C. C. Huang and J. M. Viner, *Phys. Rev. A* **25**, 3385 (1982).
- [48] A. Rapini and M. Papoular, *J. Phys. (Paris), Colloq.* **30**, C4 (1969).
- [49] S. Kralj and V. Popa-Nita, *Eur. Phys. J. E* **14**, 115 (2004).
- [50] P. Poulin and D. A. Weitz, *Phys. Rev. E* **57**, 626 (1998).
- [51] Z. Bradač, S. Kralj, M. Svetec, and S. Žumer, *Phys. Rev. E* **67**, 050702(R) (2003).
- [52] P. Poulin, V. Cabuil, and D. A. Weitz, *Phys. Rev. Lett.* **79**, 4862 (1997).
- [53] J. Chakrabarti, *Phys. Rev. Lett.* **81**, 385 (1998).
- [54] N. Leon, J. P. Korb, I. Bonalde, and P. Levitz, *Phys. Rev. Lett.* **92**, 195504 (2004).
- [55] N. Vaupotič, S. Kralj, M. Čopič, and T. J. Sluckin, *Phys. Rev. E* **54**, 3783 (1996).
- [56] L. Benguigui and P. Martinoty, *Phys. Rev. Lett.* **63**, 774 (1989).